Performance evaluation of symmetric and non-symmetric geometrical layouts of the Astroneu array

A. Leisos[a,*], T. Avgitas[a,b], G. Bourlis[a], G. K. Fanourakis[c], I. Gkialas[d], A. Stamelakis[a], I. Manthos[d], A. G. Tsirigotis[a] and S. E. Tzamarias[f].

[a] *Physics Laboratory, School of Science & Technology, Hellenic Open University, Patras, Greece*

[b] *Laboratory APC, University Paris Diderot, Paris VII, Paris, France*

[c] *Institute of Nuclear and Particle Physics, NCSR Demokritos, Athens, Greece*

[d] *Department of Financial and Management Engineering, University of the Aegean, Chios, Greece*

[e] *Department of Physics, Aristotle University of Thessaloniki, Thessaloniki, Greece*

**e-mail: leisos@eap.gr*

Abstract−The Astroneu array is a hybrid air shower telescope operating at the Hellenic Open University campus detecting Extensive Air Showers (EAS). The array consists of three detection stations each comprising three large particle detectors and one radio frequency (RF) antenna. The degree of the azimuthal symmetry of a station affects the EAS detection rate, the reconstruction energy threshold, as well as the angular resolution in estimating the direction of the EAS axis. In order to study these effects the stations of the Astroneu array followed different geometrical layouts, where two of the stations exhibited azimuthal symmetry, forming an almost equilateral triangle, while another station was much asymmetric following a very elongated geometrical layout. In this work we present results based on data collected by the particle detectors of the array during a period of about eighteen months. The three stations were selecting events at average rates of 17.5, 11.5 and 18.9 showers per hour, resulting in a total number of more than 600000 reconstructed showers in the aforementioned operational period. Using detailed simulation to describe the detector effects, the EAS detection rate and the angular direction are compared to phenomenological models and the performance of each station of the telescope is evaluated. The resolution in reconstructing the angular direction by a single station is found to vary between 3 to 5 degrees, while the energy threshold for reconstructing an EAS with a single station is estimated to be 20-30 TeV both depending on the station geometry.

Keywords-Cosmic Rays, Extensive Air Showers, Scintillator Detectors, Astroneu

1. INTRODUCTION

The Astroneu array [1] is a hybrid detection system operating at the Hellenic Open University campus. In the initial phase of operation, 9 particle detectors and 3 Codalema [2] butterfly antennas [3] were installed and operated at the site. The particle detectors of each station are large scintillator counters (Scintillator Detector Module- SDM), positioned in triangle geometry following the architecture of the HEllenic LYceum Cosmic Observatories Network (HELYCON) [4] project. The typical distance between the scintillator detectors of a station is about 25 meters with an RF antenna positioned at the center of each station. An approximate equilateral triangle is formed in stations A and C, while station B forms an amblygonal triangle, offering the opportunity to study the efficiency and resolution of such geometry. The layout of the Astroneu array and details of the detector deployment are shown in Fig. 1.

Fig. 1. The Astroneu array installed at the Hellenic Open University campus. The position of the scintillator detectors are marked with squares, while the positions of the RF antennas with circles. The geodesic coordinates of the stations centers are: Station A (38°12'22.69’’N, 21°45'52.60"E), Station B (38°12'22.49"N, 21°45'59.32"E), Station C (38°12'29.62"N, 21°45'42.36"E). The top inset photo shows the arrangement of scintillation tiles and fiber optics of a particle detector. On the bottom inset photo the Codalema butterfly antenna is shown on the foreground and a particle detector on the background.

Each station is operated independently by each own Data Acquisition (DAQ) system [1]. The data selection and digitization are performed by the Quarknet board [5]. The data selection trigger is based upon a 3-fold coincidence of the particle detectors' signals, which exceed a preselected threshold of 9.7 mV; around twice the pulse height of a MIP (Minimum Ionizing Particle). The time window for the coincidence is adjusted to take into account the distances between the detectors (typically 150 ns). Each time such a coincidence occurs, the DAQ system produces a NIM pulse (Quarknet-OUT) that triggers the RF antenna of the station. Quarknet-OUT is produced with an equal probable time jitter in a window of 10 ns. Both the Quarknet board and the antenna system are equipped with GPS receivers for time tagging the recorded events. As published elsewhere [6-9] this time tagging allows for offline event selection related to EAS detected by more than one component of the array.

In this work, we present results using data collected by the particle detectors of the array, for a running period of approximately 18 months. These data sum up to a total of more than 600000 events collected by the three autonomous stations. Data are analyzed in order to evaluate the performance of each single station of the array individually. Results on the multiple station performance i.e. events that are reconstructed by more than one station, as well as the analysis of the RF signals are reported in [6-9].

The paper is organized as follows: In Section 2, we briefly outline the simulation framework and the selection of events for offline analysis. In Section 3 we describe the data analysis procedures and we present the comparison of experimental measurements with simulations and phenomenological model predictions. In Section 4 we evaluate the efficiency and resolution of a single autonomous station. Finally, in Section 5 the conclusions are drawn.

2. SIMULATION FRAMEWORK AND EVENT SELECTION

The simulation of the response of an autonomous station to cosmic rays is a two-step process; the first step concerns the phenomenology of the primary cosmic ray composition, direction, energy distribution and shower development in the atmosphere, while the second step is related to the processes involved in the experimental signal generation. Specifically, the CORSIKA [10] simulation package describes the evolution of the EAS, down to the detector level. The QGSJET-II-04 [11] and GEISHA [12] packages have been employed for high and low energy hadronic interactions respectively and the EGS4 Code system [13] for the electromagnetic interactions. For the primary particles energy, direction and composition, the model [14] was used [14] and the atmosphere was modeled using the Atmospheric model 7 of Corsika, which corresponds to the central European atmosphere for Oct. 14, 1993. We have simulated 2 10^8 EAS with primary particle energy in the range 10^{13} – 5 10^{15} eV and 10^5 EAS between 5 10^{15} and 10^{18} eV, registering the energy and the arrival direction of the primary particle initiating the shower.

Furthermore, for each simulated shower, the position coordinates and the arrival times of the EAS secondary particles at the detector level were recorded.

In the second simulation step, the Hellenic Open University Reconstruction and Simulation (HOURS) package [15-17] was employed to simulate the response of the detectors to EAS particles. This includes the interaction of the shower secondary particles with the detector material, the production of scintillation light, the transmission through the optical fibers, the photomultiplier response, the signal propagation and attenuation through the cable, as well as the digitization and trigger formation [1].

In order to use efficiently the CORSIKA EAS simulations, each simulated shower was sampled more than once, by moving the impact point of the shower axis to the ground uniformly, around the center of each station[1] and selecting appropriately the secondary particles, which fall within the particle detectors effective area.

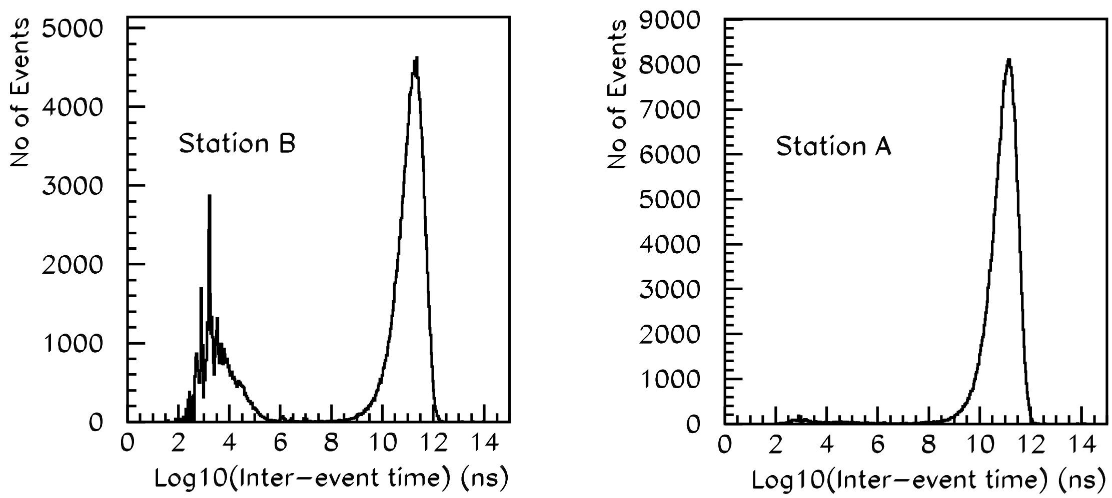

Fig. 2. Distribution of time difference, in logarithmic time scale, between consecutive events. The different behavior on station B is due to the noise clusters.

The identification and rejection of events caused by noise is of crucial importance, especially in station B, which has been deployed next to a strong noise source (air conditioning system). As depicted in Fig. 2, triggers caused by environmental electronic noise appear in clusters of very small time intervals between successive events. Thus, event clusters with inter-event time separation less than 0.1 s were rejected.

---

[1] Inside a disk with radius of 420 m, since beyond this area only very high energy showers are detectable which, however, constitute a negligible fraction of the detected EAS.

Station	A	B	C
No of triggers	338658	245275	368804
No of selected events	226269	116850	249570
Operating period (h)	12946	10123	13222

Tab. 1. Number of experimentally selected events in each station before and after the application of noise rejection. The effect of the selection criteria in station B, clearly shows the increased noise level already mentioned and depicted in Fig. 2. Additionally, the operating period of each station is presented.

As described in [1] the Quarknet electronics digitize the times when the rising and falling edges of the detector-signal waveforms cross a predefined threshold. Another criterion to reject noise is based on the requirement that consecutive digitizations related to the same waveform should correspond to alternating rising and falling edges. Unexpected sequences (e.g. a rising edge following a rising edge) were rejected, while the remaining rising/falling edges were considered as candidate pulses. In the most of the cases only one candidate pulse is found per waveform. Otherwise the surviving candidate pulses were merged if all the following conditions were met: a) merging was performed only within a time window of 500 ns in order to avoid the effect of cable reflections, b) only following smaller pulses were incorporated to bigger pulses and c) the time difference between successive pulses was smaller than 30 ns. If after merging more than one candidate pulses were remained, only the first pulse was used in the subsequent steps of the analysis. The leading edge digitization (i.e. the time when the rising edge of the waveform crosses the preselected voltage threshold) corrected for time delays introduced by the electronics, cables etc., provides the signal arrival time. Pulses with a time difference between the leading and the falling edge digitizations (hereafter called Time Over Threshold, *ToT*) less than 15 ns were rejected. Following the above merging and cleaning of the individual detector signals, the event trigger selection criteria were reapplied to the surviving pulses. The numbers of events fulfilling the above selection criteria (hereafter selected events) are listed in Tab. 1 together with the number of triggers and the respective operating time. The event selection rates were found to be 17.5 ± 0.3, 11.5 ± 0.3, 18.9 ± 0.3 events per hour for stations A, B and C respectively, which are consisted with the expected rates taking into account the geometrical acceptances as it is discussed in Section 4.

3. DATA ANALYSIS

In the following analysis, the timing of the rising edge (hereafter pulse timing) and the *ToT* of each detector signal were used to provide information related to the shower-front arrival time and to the secondary particles density at the detector position, respectively.

The relative pulse timing of the three detector signals is used to determine the shower direction (zenith and azimuth angle of the shower axis). Such a timing method, i.e. using a constant discrimination threshold, suffers from systematic bias (slewing) which depends on the amplitude of the signal. In this analysis the *ToT* measurement is used to correct the pulse timing for such systematic slewing. As it is described in detail in [18], we have used the simulation to evaluate the mean systematic slewing, $\Delta(T_H)$, as a function of the related *ToT* value, T_H, determined at the threshold level H. It has been checked that after subtracting the slewing systematic from the pulse timing, t_M, (i.e. $t_R=t_M-\Delta(T_H)$) the corrected timing, t_R, for pulses with *ToT* values in a narrow interval of T_H follows a Gaussian distribution with a mean value equal to the true pulse arriving time and sigma $\sigma(T_H)$, which has been parameterized as a function of the T_H. In [18] the above parameterizations have been validated using calibration data collected in special detector deployments and found to describe very well the detector timing characteristics.

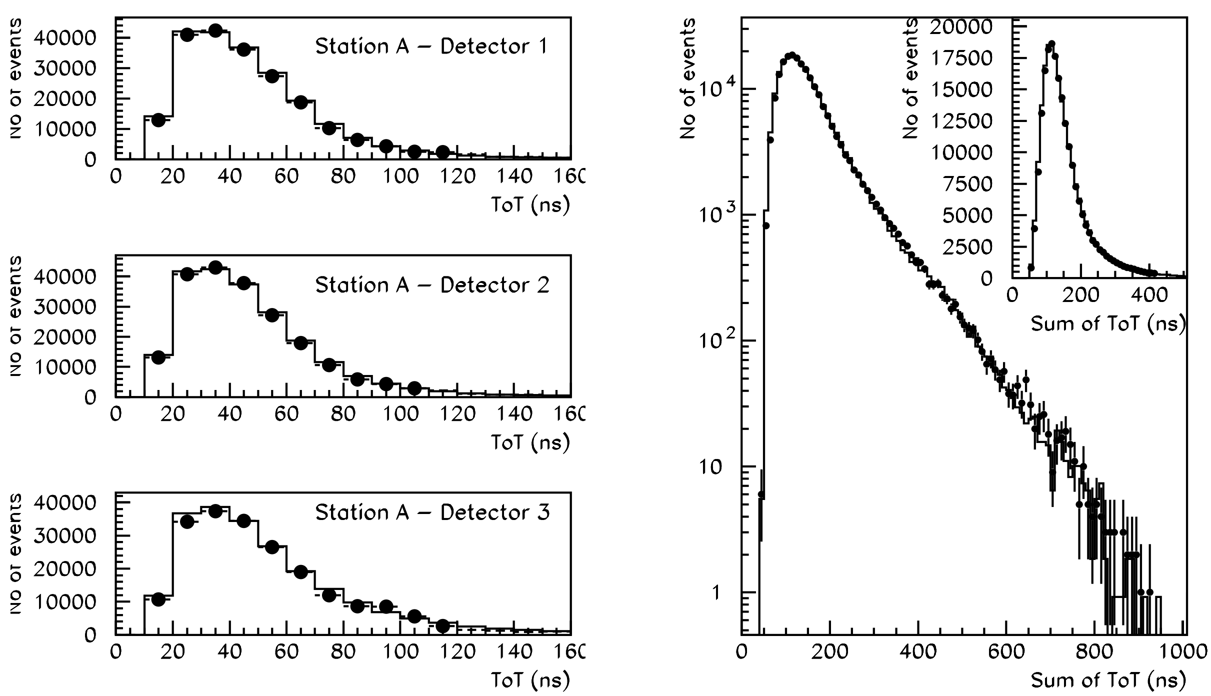

Fig. 3. Left: Distribution of the *ToT* values for each detector of station A, for experimental data (dots) and MC estimation (histogram), normalized to the operation time of the detecting station. (Right) The sum of the three *ToT* values for each event in semi-log scale, for experimental data

(dots) in comparison with MC simulation (histogram) normalized to the operation time of the detecting station. Same plot in linear scale appears in the inset plot.

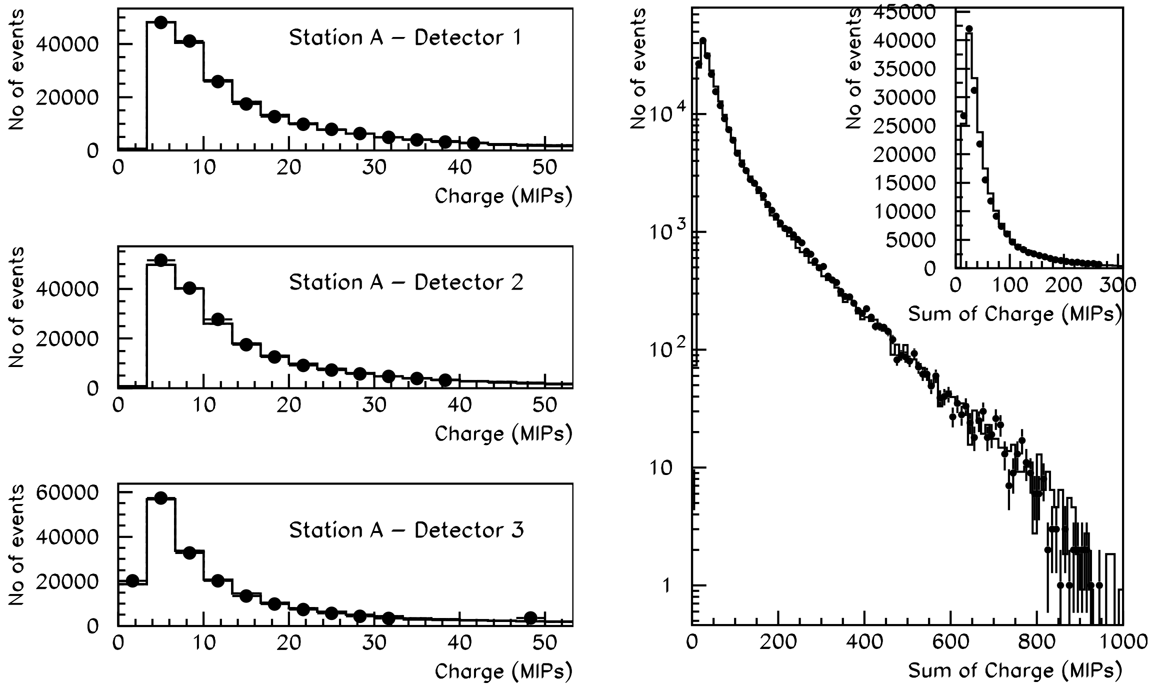

Fig. 4. Left: Distribution of the charge of each detector of station A, as estimated from the experimental data using charge versus *ToT* parameterization provided by the simulation (dots). The histogram represents the same distribution as predicted by the simulation, by integrating the full-simulated waveforms and normalizing to the detector operation time. Right: Distribution of the sum of the charge of the three detectors for each event in semi-log scale, estimated from the experimental measurements (dots) in comparison with the full-simulation prediction (histogram). Same plot in linear scale appears in the inset. The charge is in units of the MIP equivalent charge.

The success of employing the *ToT* measurement for correcting systematic timing-biases relies on the information content of the *ToT* measurement related to the size (charge or amplitude) of the pulse. However, the utilization of the above method depends on the success of the simulation to describe the detector response to showers and especially to describe the signal characteristics that are related to *ToT*. The performance of the simulation has been validated in detail using calibration data [18] and similar very good agreement between experimental data and simulation has been found in shower events. As a demonstration, in Fig. 3, the distribution of the *ToT* measurement by each detector (left) and the distribution of the sum of the *ToT* values of all three detectors of station A (right) are shown in a very good agreement with the simulation predictions. Furthermore, the very good performance of the simulation to describe the detector response allows the expression of several pulse properties as functions of the related *ToT* and the utilization of the *ToT* measurements in order to estimate pulse characteristics that are not available from direct measurements. For example, in Fig. 4 it is shown the distribution of the charge of the detector signal as it has been estimated from the data using *ToT* measurements in a very good agreement with the simulation prediction.

Close to ground level, at any given moment, the EAS particles are distributed around a curved surface (hereafter called EAS particle-front). Due to the limited inter-detector distance of the Astroneu stations, only a part of the EAS particle-front is detected (hereafter called local shower-front) by a single station. The local shower-front can be adequately approximated as a plane moving parallel to itself with the speed of light. The direction of its movement, i.e. the zenith and azimuth directional angles of an axis perpendicular to the local particle-front, is evaluated using the available experimental information. Specifically, the SDM signal arrival time is used as an estimation of the time when the EAS local particle-front arrives at the center of the respective detector. Then the direction of movement (hereafter called reconstructed shower direction) is evaluated by the relative timing between the SDM signals of the station and the related detector positions (hereafter called triangulation method).

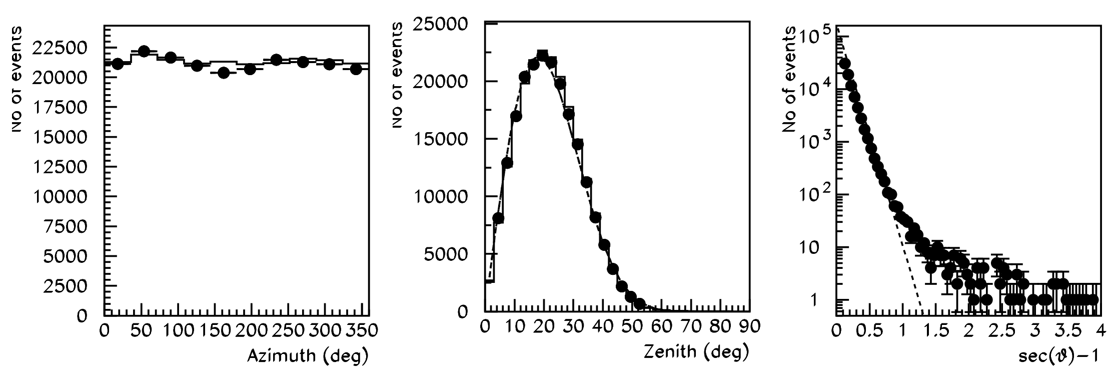

Fig. 5. Distributions of the zenith (left) and azimuth (middle) angles of the reconstructed direction of EAS local shower-front for station A. The experimental data are represented with dots, while the MC prediction with the histogram. On the right plot the distribution of secθ-1 is shown. The distribution for $\theta<45^o$ is well fitted ($p(\chi^2)=0.61$) with exponential function of the form $e^{11.54-9.68\,(\sec\theta-1)}$.

Distributions related to the reconstruction of the detected EAS local particle-fronts are shown in Fig. 5, in a very good agreement with the MC predictions. The data points correspond to the reconstructed direction of EAS detected by station A[2], while the histograms represent MC predictions based on simulated showers treated the same way as the experimental data. Specifically, the azimuth angle of detected and reconstructed EAS follows an almost equal-probable distribution (see also Section 4), while the zenith angle distribution is well approximated by the following parametric form:

$$\frac{dN}{dcos\theta} \sim cos\theta^{\alpha}, \qquad (1)$$

with spectral index, α=9.37 ± 0.04. Another parameterization of the zenith angle distribution relies on the dependence of the EAS flux on secθ according to the formula $ln\Phi = C\ sec\theta + D$ [19,20]. This parameterization is considered to be valid for zenith angles less than 45^o and the slope of the distribution equals to $-X_0/\Lambda$ where X_0 is the atmospheric depth and Λ the EAS absorption length. In Fig. 5 (Right) is shown the secθ-1 distribution fitted with exponential function resulting to Λ=107 g/cm^2 in agreement with other measurements at sea level [21-24].

4. PERFORMANCE OF THE ASTRONEU STATION

The limited size of the current Astroneu array does not allow the reconstruction of the global EAS characteristics, i.e. the impact point of the global EAS axis and the energy of the primary particle. However, as demonstrated in the previous Sections, the MC simulation chain results to predictions which describe very well the observed functionality of the Astroneu stations as well as the measurements concerning the direction of the local shower-front. Motivated by this agreement, the full simulation chain was utilized to study the efficiency and resolution of the Astroneu stations concerning the reconstruction of the local shower-front as well as the dependence of the station performance on the energy of the primary particle and the proximity of the EAS axis at the ground level to the center of the station (hereafter called proximity distance or just distance).

Using MC simulated events the statistical error (hereafter called resolution) in estimating a directional angle (zenith, azimuth) of the primary particle was defined as the square root of the variance of the difference between the true angle of the EAS primary particle and the respective reconstructed angle of the EAS local shower-front. Similarly, the 3D-error in estimating the

---

[2] The same good agreement between the measured angular distributions and the MC predictions is also found in the data collected with the rest of the Astroneu stations.

direction of the primary particle was defined as the median of the distribution of the 3D-angle between the primary particle direction and the reconstructed direction of the local shower-front.

Fig. 6 demonstrates the performance of an Astroneu station in reconstructing the direction of the EAS primary particle. The left-column plots present the resolution in reconstructing the zenith angle, the middle-column plots the resolution in reconstructing the azimuth angle and the right-column plots present the 3D-error in reconstructing the primary particle direction.

A more accurate timing directional reconstruction is expected for showers passing close to the station center than showers passing through larger distances. Indeed, when the global shower axis passes through (or very close to) the station, the axis of the local shower-front is almost the same with the direction of the primary particle. Furthermore, the showers passing close to the center of the station are expected to induce strong signals in the detectors resulting to precise timing measurements [18]. This is demonstrated in the top-row plots of Fig. 6.

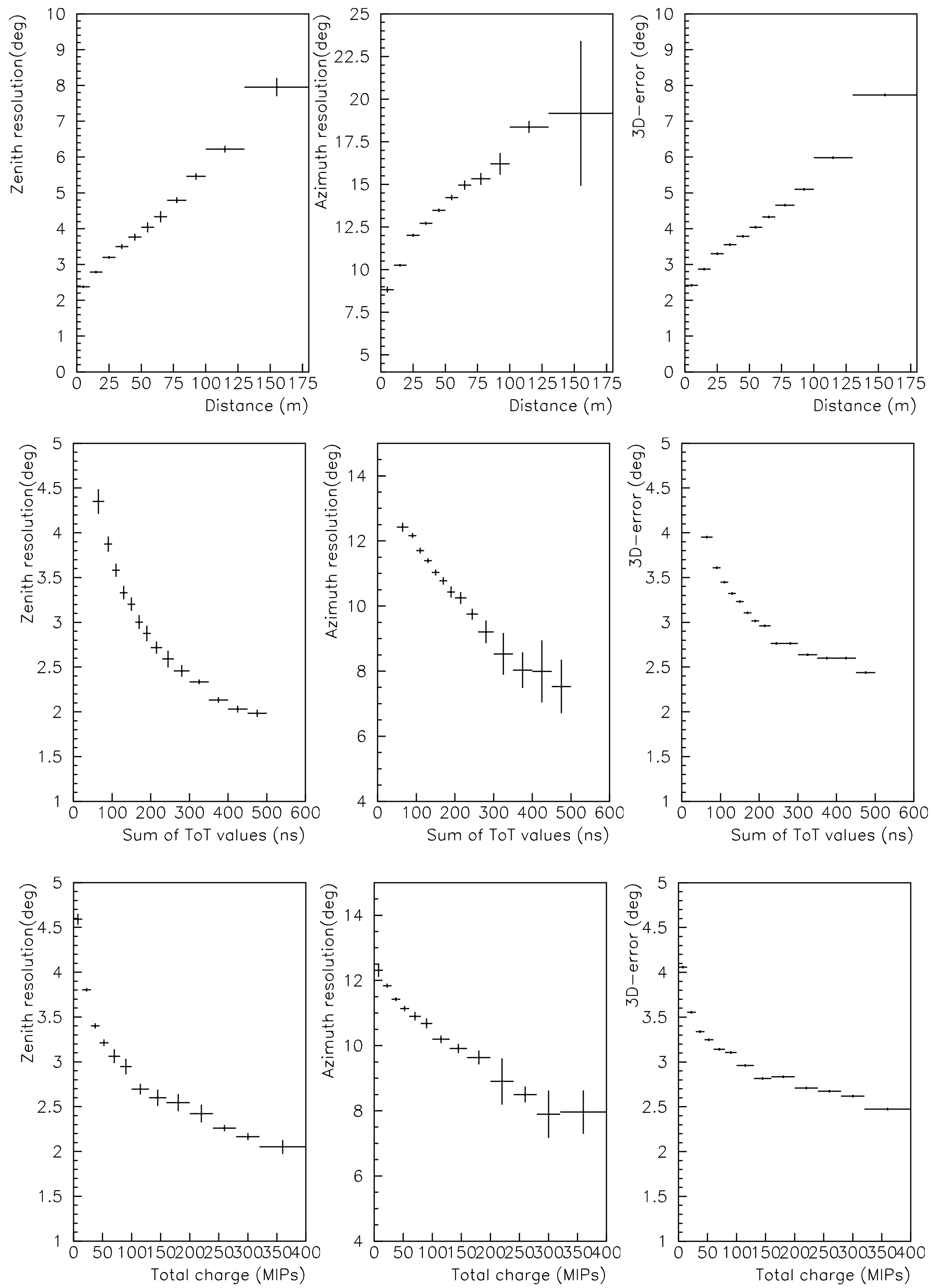

Fig. 6. Resolution of the zenith (left column), of the azimuth angle estimation (middle column) and the 3D-error between true and reconstructed direction of the shower (right column), versus the distance of the EAS axis impact point from the center of the station (top row), the total *ToT* (sum of the *ToT* of the three detectors) (center row) and the sum of the charge of the three detector signals (bottom row).

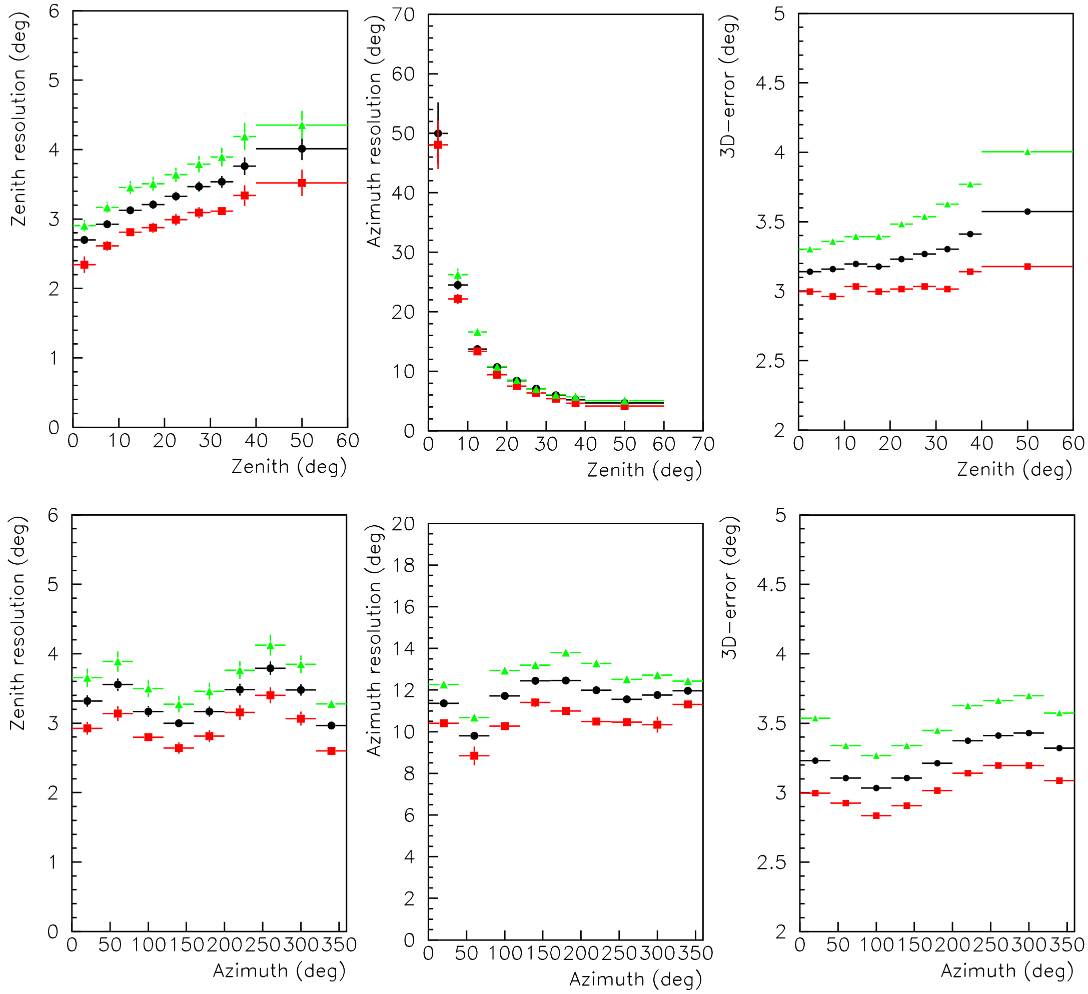

Fig. 7. Error of the zenith angle (left), error of the azimuth angle estimation (middle) and median angle between true and reconstructed direction of the shower (right), versus the zenith angle (top) and the azimuth angle of the EAS (bottom) for a station with a symmetric geometrical layout as the Astroneu station A. The black circles correspond to all shower events, while the red squares (green triangles) correspond to shower events with collected charge more (less) than the median of the total charge distribution.

For the same reasons as above, it is expected that the accuracy in reconstructing the shower direction, depends strongly on the strength of the signal induced by the shower particles to the detectors of the station. This effect is also demonstrated in the bottom row of Fig. 6 where the reconstruction accuracy is shown as a function of the collected (by all the three detectors of the station) total charge. However, in Astroneu the charge of the signals is estimated by using the respective *ToT* measurements [18]. The middle-row plots of Fig. 6 demonstrate the dependence of the reconstruction accuracy on the strength of the detector signals using the sum of the *ToT* measurements by each one of the three individual detectors of the station.

The accuracy in determining the shower direction depends also on the direction of the primary particle, which initiates the shower. In Fig. 7, the resolutions in reconstructing the zenith angle (left) and the azimuth angle (middle), as well as the 3D-error (right) are presented versus the zenith (top) and the azimuth (bottom) direction angles of the primary particle.

As shown in Fig. 7, the zenith angle resolution worsens, as the zenith angle of the primary particle gets larger. In principle such dependence is expected due to the fact that the statistical error in estimating the zenith direction θ by triangulation is inverse proportional to cosθ.

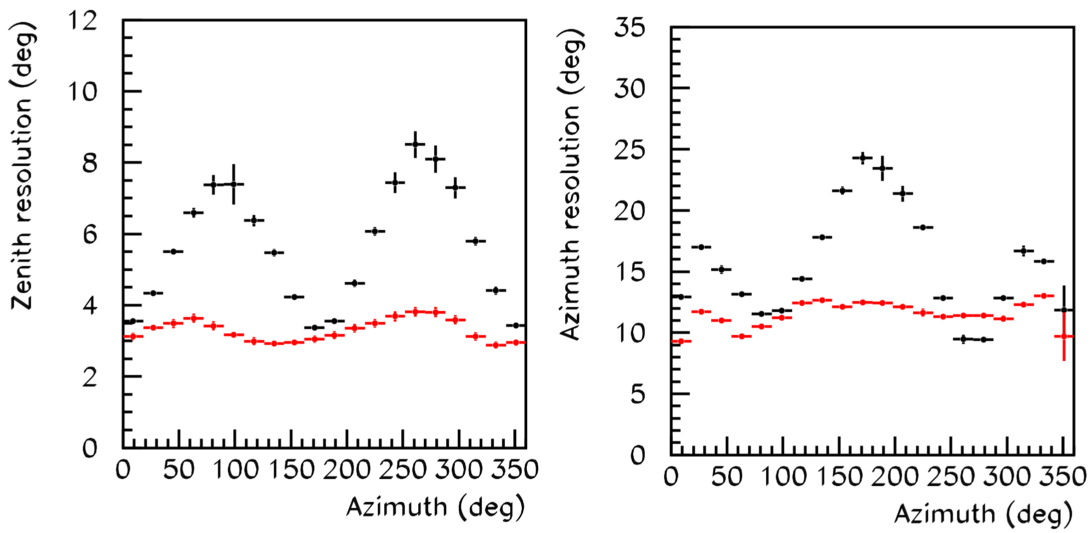

Fig. 8. Resolution in reconstructing the zenith (left) and azimuth (right) directional angles versus the azimuth angle of the incoming EAS. The black points represent the full MC simulation prediction for an asymmetric, elongated layout (station B) and the red points correspond to an almost symmetrical layout (station A).

However, the accuracy in estimating the arrival time of the particle-front at the detector position depends strongly on the strength of the induced signals on the detectors [18], which in turn depends on the shower inclination. Indeed, the effective area of an Astroneu detector, as seen by an EAS particle-front, is proportional to cosθ. Consequently, inclined showers will induce weaker signals on the detectors, relative to the signals induced by vertically coming showers.

Moreover, the particle density of the shower-front on the detectors level depends on the zenith angle, since inclined showers have to go through larger distances in the atmosphere before reaching ground. Both the above-mentioned effects result to lower induced signals to the detectors, causing poorer reconstruction accuracy at large zenith angles. This effect is also demonstrated in Fig. 7 (top row) by comparing the expected reconstruction accuracies, versus the zenith angle, of EAS that induce detector signals of different strength (see the figure caption).

Considering the accuracy in estimating the azimuth angle by triangulation, an improvement inversely proportional to sinθ is expected, which is demonstrated by this MC study. As it is also shown in Fig. 7 (top middle) the $\sin^{-1}\theta$ dependence has a much greater impact to the azimuth resolution than the previously mentioned effect on the resolution, caused by the signal strength reduction due to the inclination of the shower.

Since an Astroneu station comprises 3 detector units, even if they were deployed in an equilateral triangle, the resolution of estimating the direction of a detected EAS is a function of the azimuth angle of the incoming shower. This is due to the fact, that the directional angles, as determined by triangulation, depend on the relative direction of the horizontal component of the shower axis vector with respect to the inter-detector segments. Such a deviation from a uniform resolution versus the azimuth angle of the detected shower is demonstrated in Fig. 7 (bottom row). The deviation from uniformity depends on the geometrical layout of the detectors, as it is shown in Fig. 8 (top) for the case of an asymmetrical, elongated detector deployment (station B).

The dependence of the 3D-error on the zenith and azimuth directional angles of the EAS is also shown in Fig. 7. Fig. 9 (left) shows the 3D-angle between the direction of the primary particle and the reconstructed direction of the local particle-front, in case of a symmetric geometrical layout as the Astroneu station A. The 3D-error in the above distribution is 3.25 degrees. However as shown in Tab. 2 the reconstruction error depends on the geometrical layout of the station (inter-detector distance and symmetry).

The station efficiency in detecting EAS depends on the energy (hereafter called EAS energy), on the inclination of the primary particle, as well as on the proximity distance of the shower axis. The direction of the primary particles (see also Section 2) follows an equal-probable distribution with respect to the cosine of the zenith angle, as well as with respect to the azimuth angle. However, the detection process biases the zenith distribution of the reconstructed showers (see Fig. 5) to lower zenith angles, due to the fact that the atmospheric absorption is larger for inclined showers. Nevertheless, such absorption is independent of the azimuth angle of the primary particle as it is demonstrated by the almost flat azimuth angle distribution of the reconstructed showers shown in Fig. 5.

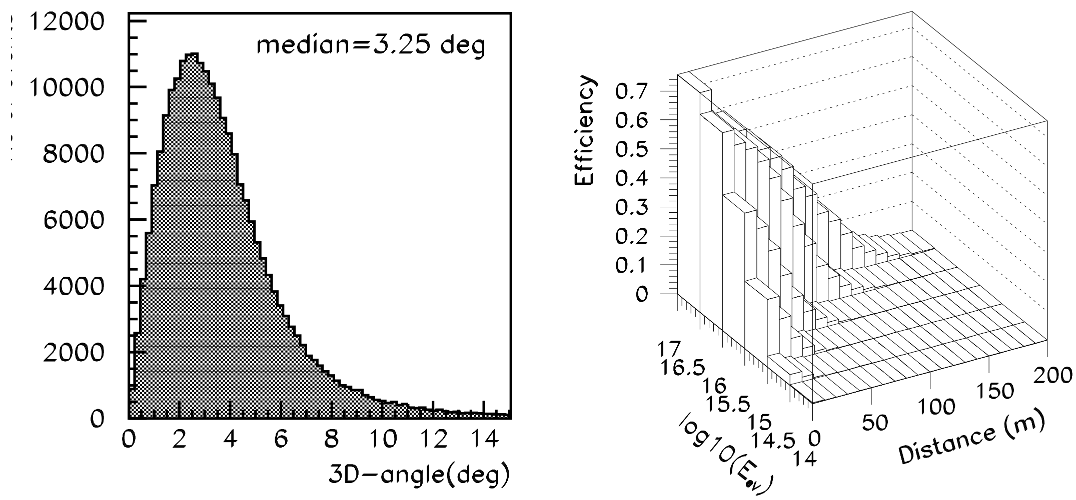

Fig. 9. The 3D-angle between the direction of the primary particle and the reconstructed direction of the local shower-front, for a symmetric station following the geometrical layout of the Astroneu station A. (right) The reconstruction efficiency as a function of the EAS proximity distance and the energy of the primary particle. The last bin in energy includes energies with log(E_{eV})>16.5.

The dependence of the detection efficiency of station A on the proximity distance and on the EAS energy, is presented in Fig. 9 (right). At low distances and at very high EAS energies the efficiency exceeds 70%, falling for larger proximity distances and lower energies. However, the detection efficiency depends on the geometrical layout and the operational parameters of the Astroneu stations. The efficiency performance of the symmetric station C is very similar to the station A and both are able to reconstruct showers of energies as low as 20 TeV at low proximity distances. On the other hand, the reconstruction efficiency of station B, which follows an elongated geometrical layout, does not exceed 30% at very high energies and its energy reconstruction threshold is more than 30 TeV. Furthermore, since station B operates at high noise environment, tighter selection criteria are applied to the recorded signals, resulting to a much lower reconstructed EAS rate than the other stations. The performance parameters of the Astroneu stations are summarized in Tab. 2.

Station	EAS Reconstruction Rate (hr^{-1})	σ_θ (deg)	σ_φ (deg)	ω (deg)	E_{th} (TeV)
A	17.5 ± 0.3 (16.8)	3.3	10.4	3.3	20
B	11.5 ± 0.3 (11.9)	6.0	14.8	5.5	30
C	18.9 ± 0.3 (18.7)	3.7	11.2	3.6	20

Tab. 2. Parameters describing the performance of the Astroneu stations at single mode of operation. The quoted reconstructed EAS rates are based on measurements, while the numbers in parenthesis denote the simulation predictions. The errors on the measured rates are mainly due to the uncertainty of the threshold value of each channel of the Quarknet card. The resolution in reconstructing the zenith angle (σ_θ), the azimuth angle (σ_φ), the 3D reconstruction error (ω), as well as the energy threshold (E_{th}) for an EAS to be reconstructed, have been estimated by the simulation study described in the text.

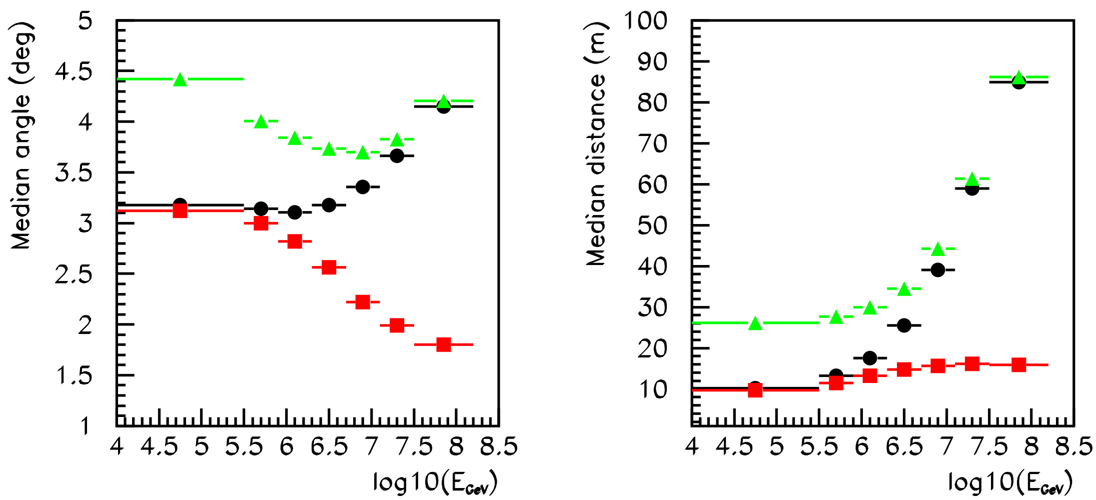

Fig. 10. Simulation results concerning the performance of an Astroneu station with the geometrical layout of station A: The 3D-error (left) and the median of the proximity distance (right) of the detected shower to the center of the station, versus the energy of the EAS primary particle. The black solid circles represent results based on the whole sample of reconstructed EAS, while the red squares and the green triangles represent results based on selected samples where the shower axis proximity to the station center is less or more than 22.8 m respectively (see text).

Fig. 10 shows the dependence of the 3D-error on the energy of the EAS primary particle. The black points correspond to all detected EAS independently of the proximity distance to the station. This dependence is also shown for EAS with the shower axis passing through (near-passing) or outside (far-passing) a disk of 22.8 m radius around the station center, which is the median of the proximity distance distribution of all the detected EAS by this station. The reconstruction error for near-passing EAS (red squares) decreases as the energy of the primary particle increases. Near-passing, high energy EAS induce strong signals at the detectors which are timed with high accuracy. Moreover, in this case the planar particle-front assumption provides a good approximation of the shower axis. The same trend is followed by the far-passing detected EAS up to energies of about $10^{6.5}$ GeV; however, for higher energies the reconstruction resolution worsens. This is due to the fact that the median distance of far-passing showers, practically after $10^{6.5}$ GeV, increases exponentially with the energy as it is demonstrated in the right plot (green triangles) of Fig. 10. As the distance of the detected showers gets larger, the effect of the shower-front curvature on the directional reconstruction becomes significant. Furthermore, at large distances, the induced weak signals on the detectors by the fringes of the shower-front suffer from larger timing errors, which also affect the reconstruction resolution. As it is also shown in Fig. 10 (black circles) there is a strong correlation between the energy dependence of the 3D-error in reconstructing the direction of any shower and the spatial distribution of the detected EAS around the station center.

5. CONCLUSIONS

The results on the performance of the Astroneu extensive air shower array, in single station operation mode are presented for a running period of 18 months. The data sample comprised more than 600,000 detected EAS allowing for a detail study of the event selection, reconstruction algorithms and performance of the stations. The detected and reconstructed EAS rates as well as several important distributions concerning the processing of the detector signals and the reconstruction of the detected EAS direction were compared and found in a very good agreement with the predictions of a detailed simulation package. In addition, the zenith distribution of the detected showers was used for the measurement of the EAS absorption length, which was found to be Λ=107 g/cm^2 in agreement with other measurements at sea level. The dependence of the detection efficiency and the reconstruction resolution were studied as functions of the EAS proximity distance, the energy and direction of the primary particle. The 3D-errors (and the reconstruction energy threshold) were found to be 3.3^o (20 TeV), 5.5^o (30 TeV) and 3.6^o (20 TeV) for the station A, B and C respectively, depending mainly on the geometrical layout of each station. The reconstructed EAS rates were found to be 17.5, 11.5 and 18.9 events per hour for the stations A, B and C respectively, depending also on the geometrical layout and the operational conditions of each station, in a very good agreement with the simulation predictions.

ACKNOWLEDGMENTS

This research has been co-financed by the European Union (European Social Fund - ESF) and Greek national funds through the Operational Program "Education and Lifelong Learning" of the National Strategic Reference Framework (NSRF) - Research Funding Program: "THALIS - Hellenic Open University - Development and Applications of Novel Instrumentation and Experimental Methods in Astroparticle Physics" and by the Hellenic Open University Grant No. ΦΚ 228.

REFERENCES

1. Avgitas, T., Bourlis G, Fanourakis G.K., Gkialas I., Leisos A., Manthos I., Tsirigotis A.G. and Tzamarias S., *JINST*, 2020, vol. 15, T03003. https://doi.org/10.1088/1748-0221/15/03/T03003

2. D. Ardouin et al, Radio-detection signature of high-energy cosmic rays by the CODALEMA experiment, Nucl. Instrum. Methods A, 555:148163, 2005.

3. D. Charrier et al, Antenna development for astroparticle and radioastronomy experiments, Nucl. Instrum. Methods Phys. Res. Sect. A 2012, 662, S142--S145.

4. A. Leisos et al, Hellenic Lyceum Cosmic Observatories Network: Status Report and Outreach Activities, Universe 2019, 5(1), 4; https://doi.org/10.3390/universe5010004

5. S. Hansen et al, Low-cost data acquisition card for school-network cosmic ray detectors, IEEE Transactions on Nuclear Science, Volume 51, Issue: 3 (2004), pages 926-930

6. A. Leisos et al, Detection of high energy showers by the Astroneu extensive air shower array, New Astronomy,Volume 82, 2021,101448, https://doi.org/10.1016/j.newast.2020.101448

7. I. Manthos et al, Cosmic Ray RF detection with the Astroneu array, New Astronomy 2020 101443, https://doi.org/10.1016/j.newast.2020.101443

8. A. Leisos et al, Hybrid detection of high energy air showers in urban environments, MDPI, Universe 2019, 5(1), 3

9. S. Nonis et al, Angular reconstruction of high energy air showers using the radio signal spectrum, 2020 Phys. Scr. 95 084007,https://doi.org/10.1088/1402-4896/ab9f79

10. D. Heck et al, CORSIKA: A Monte Carlo code to simulate extensive air showers, Forschungszentrum Karlsruhe Report, (1998)

11. S. Ostapchenko, Monte Carlo treatment of hadronic interactions in enhanced Pomeron scheme: QGSJET-II model, Phys. Rev. D, 2011, 83: 014018.

12. H. Fesefeldt, Simulation of hadronic showers, physics and applications, Technical report PYTHA 85-02, III Physikalisches Institut, RWTH Aachen Physikzentrum, 5100 Aachen, Germany, September 1985.

13. W. R. Nelson et al, "The EGS4 Code System". Report SLAC265, Stanford Linear Accelerator Center, Stanford, California, 1985.

14. B. Wiebel-Sooth, P. L. Biermann: Landolt-Börnstein, Cosmic Rays, vol. VI/3c, Springer Verlag 1999.

15. A. G. Tsirigotis et al, HOU Reconstruction and Simulation (HOURS): A complete simulation and reconstruction package for very large volume underwater neutrino telescopes, Nucl. Instrum. Methods A 2011, 626, S185--S187.

16. A. G. Tsirigotis et al, Reconstruction efficiency and discovery potential of a Mediterranean neutrino telescope: A simulation study using the Hellenic Open University Reconstruction and Simulation (HOURS) package, Nucl. Instrum. Methods A 2013, 725, 68--71.

17. A. G. Tsirigotis et al, Hellenic Open University Reconstruction and Simulation (HOURS) software package: User Guide and short reference of Event Generation, Cherenkov photon production and Optical Module simulation, arXiv:1702.00945 [astro-ph.IM]

18. S. Tzamarias et al., Calibration procedures for accurate timing and directional reconstruction of EAS particle-fronts with Astroneu stations, Instrum Exp Tech 64, 127–140 (2021), https://doi.org/10.1134/S0020441220060202

19. Kalmykov N N, Fomin Yu A and Khristiansen G B 1973 Proc. 13th ICRC, Denuer 4 2633

20. D Ciampa and R W Clay 1988 J. Phys. G: Nucl. Phys. 14 787

21. A.M. Elo and H. Arvela, Proceedings of ICRC 2001: 598 c Copernicus Gesellschaft 2001

22. Sun L. and Winn M. M., A small cosmic ray air shower array using plastic scintillators and a NIM/CAMAC recording system, Nucl. Instr. Meth. in Phys. Res., 223, 173-179, 1984

23. Zotov, M.Y., Kalmykov, N.N., Kulikov, G.V. et al. On the angular distribution extensive air showers. Moscow Univ. Phys. 64, 632?634 (2009). https://doi.org/10.3103/S0027134909060149

24. A.~Iyono, C.~Noda, H.~Matsumoto, M.~Masuda, T.~Wada, K.~Okei, T.~Nakatsuka, T.~Morita, S.~Ohara, T.~Konishi, N.~Ochi, N.~Takahashi, S.~Tsuji and I.~Yamamoto,"Zenith

Angle Distribution and Atmospheric Effect for EAS with LAAS experiments," ICRC 2007, 47-50